Interaction of Water with Ordered θ-Al_2O_3 Ultrathin Films Grown on NiAl(100)

Emrah Ozensoy, János Szanyi,* and Charles H. F. Peden

Interfacial Chemistry and Engineering, Chemical Sciences Division, Pacific Northwest National Laboratory, P.O. Box 999, MSIN K8-93, Richland, Washington 99352

Received: November 5, 2004; In Final Form: December 8, 2004

The structure of an ordered, ultrathin θ-Al_2O_3 film grown on a NiAl(100) single-crystal surface was studied by Auger electron spectroscopy (AES), X-ray photoelectron spectroscopy (XPS), and low-energy electron diffraction (LEED), and its interaction with water was investigated with temperature programmed desorption (TPD) and XPS. Our results indicate that H_2O adsorption on the θ-Al_2O_3/NiAl(100) surface is predominantly molecular rather than dissociative. For $\theta_{H_2O} < 1$ ML (ML = monolayer), H_2O molecules were found to populate Al^{3+} cation sites to form isolated H_2O species aligned in a row along the cation sites on the oxide surface with a repulsive interaction between them. For $\theta_{H_2O} > 1$ ML, three-dimensional ice multilayers were observed to form, which then desorb during TPD with approximate zero-order kinetics as expected. A small extent of H_2O dissociation was observed to occur on the θ-Al_2O_3/NiAl(100) surface, which was attributed to the presence of a low concentration of oxygen atom vacancies. Titration of these defect sites with adsorbed H_2O molecules revealed an estimated defect density of 0.05 ML for the θ-Al_2O_3/NiAl(100) system consistent with the ordered nature of the synthesized oxide film.

1. Introduction

Metal oxide surfaces have been extensively studied due to their relevance to a vast number of materials engineering and catalytic process applications.[1−31] In particular, Al_2O_3 polymorphs have been the catalytic support of choice for various profoundly important catalytic processes such as the selective catalytic reduction (SCR) of NO_x species[1] and NO_x storage.[2] H_2O adsorption on solid metal oxide surfaces is a key step in these catalytic systems in which the nature of the interaction between water and the metal oxide surface, as well as its interaction with other reactants, dictate the fundamental reactivity and selectivity trends.

Different Al_2O_3 polymorphs can be epitaxially synthesized as thin films on NiAl bimetallic single-crystal substrates by varying the preparation protocols, by controlling the oxidation temperature and O_2 (or H_2O) pressure during the growth process.[3,4] Using this approach, a variety of transitional Al_2O_3 polymorphs can be obtained, such as amorphous Al_2O_3 films with randomly packed oxygen atoms at tetrahedral (T_h) lattice sites, a θ-Al_2O_3 structure with a monoclinic unit cell where O atoms occupy both octahedral (O_h) and T_h sites forming an fcc sublattice, a cubic γ-Al_2O_3 film with an fcc oxygen sublattice occupying T_h and O_h sites, and eventually the most stable polymorph, α-Al_2O_3, with a hexagonal unit cell and an hcp oxygen sublattice in which all of the O atoms are located at the O_h sites. It should be noted that the major difference between θ and γ polymorphs is their different relative oxygen populations at the O_h and T_h sites. For both of these Al_2O_3 polymorphs grown on NiAl single-crystal substrates, the oxide surface was suggested to be oxygen terminated with Al^{3+} cation sites located below the surface oxygen layer.[3,5−7]

NiAl(100) single crystals have a body centered cubic (bcc) structure with a stacking sequence of ABAB... where their surface displays a square unit cell. Although clean NiAl(100) surfaces can be either Ni or Al terminated under ultrahigh vacuum (UHV) conditions, in the presence of an oxidizing environment Al atoms tend to diffuse to the surface,[3,8] forming an AlO_x/Al_2O_3 layer. This process is explained by the thermodynamic stability of surface aluminum oxides with respect to the NiO counterparts as the heat of formation of Al_2O_3 is about 7 times greater than that of NiO (ΔH_f (NiO) = −240 kJ/mol).[9]

Water adsorption on metals and metal oxide surfaces has been thoroughly discussed in two separate comprehensive reviews by Thiel et al.[10] and more recently by Henderson.[11] According to these reviews, there is a strong interaction between the adsorbed water species and oxide surfaces. Commonly, at relatively low coverages, H_2O is found to adsorb molecularly on the cation sites of the oxide surface, leading to isolated water molecules lacking intermolecular hydrogen bonding. The typical adsorption configuration of H_2O to the oxide surface under these conditions involves bonding between the Lewis acid sites of the oxide (i.e., cationic sites) and the lone pair of the O atom in the water molecule. As the coverage of adsorbed water is increased, formation of hydrogen bonds interlinking originally isolated H_2O molecules is observed, which eventually results in crystalline or amorphous multilayer ice formation. On the other hand, there are also various examples in which H_2O molecules tend to adsorb dissociatively on oxide surfaces.[10,11] Dissociative adsorption of water on oxide surfaces has been generally attributed to surface defects. Indeed, on high surface area γ-Al_2O_3 powders where surface defects might be expected to be prevalent, as many as 5−7 different hydroxyl species were identified.[12]

The nature of H_2O adsorption (i.e., molecular or dissociative) on alumina surfaces seems to be closely related to the Al_2O_3 structure. Although H_2O was reported to adsorb molecularly on ordered γ-Al_2O_3/NiAl(110) thin films,[6,7] it was found to adsorb dissociatively on Al_2O_3/Al(111),[13] α-Al_2O_3(0001),[14−17] γ-Al_2O_3/NiAl(100),[4] and various transitional Al_2O_3 films grown on Ru(001).[18] In a recent study, it was also shown that H_2O

* Corresponding author. E-mail: janos.szanyi@pnl.gov.

10.1021/jp0449206 CCC: $30.25
Published on Web 02/02/2005

adsorption on ordered Al_2O_3/NiAl(110) and Al_2O_3/NiAl(100) at H_2O pressures above 10^{-5} Torr resulted in an irreversible reconstruction of the oxide surface and the loss of long-range order.[19]

In the current report, we focus on the properties of ordered θ-Al_2O_3 ultrathin films grown on a NiAl(100) single-crystal substrate whose stoichiometry, morphology, and chemical structure can be analyzed in detail with conventional surface analysis probes. Therefore, the nature of the interaction between θ-Al_2O_3 polymorphs with adsorbed H_2O can be thoroughly investigated in relevance to the structural properties of the alumina thin films.

2. Experimental Section

Experiments were performed in a UHV surface analysis chamber ($P_{base} = 3 \times 10^{-10}$ Torr) equipped with conventional surface spectroscopic probes, a high-pressure cell for IR experiments, and a Tectra ECR plasma source. The NiAl(100) single crystal used in the experiments (Princeton Scientific Corp., 10 mm diameter, 2 mm thick) was polished on both sides and spot-welded onto a U-shaped Ta wire. A C-type thermocouple was spot welded to the top edge of the crystal for temperature measurements. Cleaning of the NiAl(100) crystal was performed by alternating cycles of Ar^+ ion sputtering ($V_{beam} = 1.5$ kV, $I_{beam} = 1.5$ μA) and high-temperature UHV anneals at 1200 K. Cleanliness of the surface was checked with AES and LEED. TPD experiments were performed using a differentially pumped UTI quadruple mass spectrometer (QMS) by applying -70 V bias voltage on the spectrometer shield to constrain the ionizing electrons to the interior of the QMS shield, to prevent any possible electron beam damage on the sample. All of the TPD data presented in this study were obtained by ramping the temperature of the crystal at a 2 K/s rate, and all of the H_2O exposures were done at 100 ± 10 K sample temperature. A tubular pinhole doser, positioned in close proximity of the sample (2 mm away), was used in the adsorption experiments, which allowed the background pressure in the chamber to stay within 4×10^{-10} Torr range during the dosing processes to minimize background desorption artifacts in the TPD data. AES measurements were carried out with a beam energy of 3 kV, using a single pass cylindrical mirror analyzer (CMA, PHI-15-155) with the sample oriented normal to the AES electron gun. LEED images were acquired by employing rear-view LEED optics (PRI-155) at a beam voltage of 105 eV. XPS data were acquired with a multichannel electrostatic hemispherical analyzer (Omicron, EA-125), using a Mg Kα X-ray source ($h\nu = 1253.6$ eV). The X-ray source was oriented 50° with respect to the sample normal. XPS measurements corresponding to the H_2O adsorption experiments were also performed at 100 ± 10 K. High-purity water (Aldrich) used in the experiments was further purified by several freeze−pump−thaw cycles. Deconvolution of the XPS spectra was performed using Gaussian curves where the residual curve obtained after subtracting the fitted curves from the experimental data had peak areas equal to or less than 3% of the experimental data.

Ultrathin θ-Al_2O_3 films on NiAl(100) were grown by saturating the clean NiAl(100) surface with O_2 at 300 K (using a single O_2 dose) and by successively oxidizing the O-saturated surface at 1200 K in UHV for 30−60 min. The quality of the θ-Al_2O_3 films was checked with AES, XPS, and LEED. The thicknesses of the θ-Al_2O_3 films were estimated on the basis of the attenuation of the $Ni_{848\ eV}$ LVV AES feature associated with the NiAl(100) substrate, using the relationship:[20]

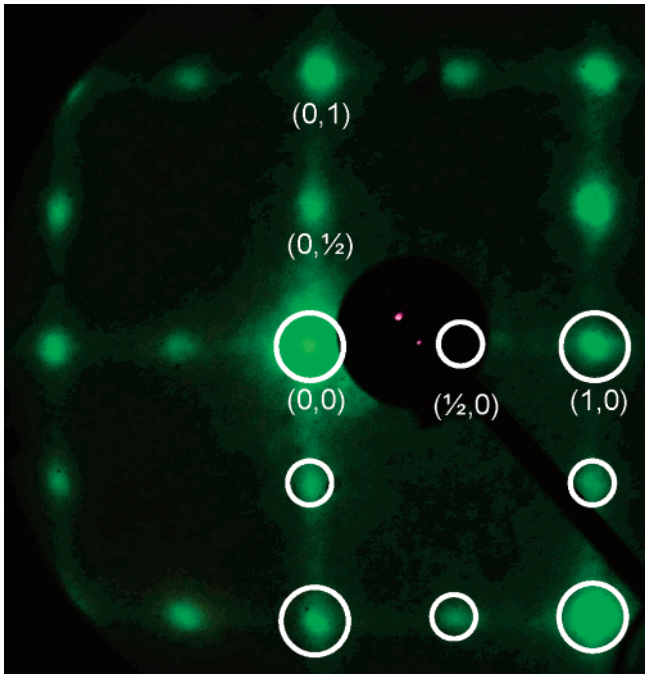

Figure 1. LEED image obtained at 105 eV for a θ-Al_2O_3/NiAl(100) surface that is synthesized using the procedure described in the text.

$$d = -\lambda_i^s \cos(\alpha) \ln(I_s/I_s^o)$$

where d is the film thickness, λ_i^s (25.88 Å) is the inelastic mean free path of electrons with a kinetic energy of 848 eV in SiO_2,[20] α is the take-off angle (42.3°) for the auger electrons that are detected by the CMA, and I_s^o and I_s are the AES intensities of the Ni_{848eV} feature for clean NiAl(100) and θ-Al_2O_3/NiAl(100) surfaces, respectively. θ-Al_2O_3 films grown using the protocol mentioned above led to a typical film thickness of 6 ± 2 Å (1−2 ML). It should be noted that similar thickness calculations based on AES measurements were also performed in the literature[3] for θ-Al_2O_3/NiAl(100) films grown with similar procedures, in which case film thickness was estimated to be 8 Å (an alternative method for thickness measurement based on HREELS measurements and theoretical modeling by the same authors revealed a value of 10 Å for these films[3]). It is also worth mentioning that thicker Al_2O_3 films have been also prepared by various groups, although these films were either polycrystalline or not highly ordered.[21−23]

3. Results and Discussion

3.1. Characterization of the Ordered θ-Al_2O_3/NiAl(100) Film. Figure 1 presents the LEED image of an ordered θ-Al_2O_3 film grown on a clean NiAl(100) single crystal. In addition to the primary LEED spots forming a square pattern, $^1/_2$ order spots are clearly visible as well in Figure 1. This characteristic LEED image was previously explained by the formation of an oxygen-terminated θ-Al_2O_3 surface structure where Al^{3+} cations are located in the underlying layer forming two different domains with a $(2 \times 1, 1 \times 2)$ structure.[3,5] It is also apparent from Figure 1 that the LEED spots possess an elliptical shape rather than a completely circular geometry, which was suggested to indicate that θ-Al_2O_3 films grown on NiAl(100) might exhibit some extent of disorder in their structure.[3,5] Scanning tunneling microscopy (STM) measurements on θ-Al_2O_3 films grown on

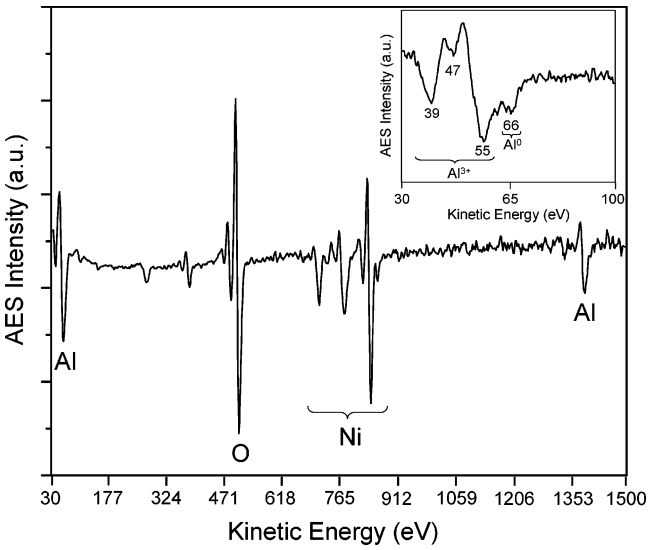

Figure 2. AES for a 6 ± 2 Å θ-Al_2O_3/NiAl(100) ultrathin film. The inset shows the detailed Auger electron spectrum corresponding to the low-energy Al feature in the main figure.

NiAl(100) reveal that θ-Al_2O_3 films develop in the form of stripes at the early stages of the film growth, eventually forming alumina domains with a combination of 3 Å high single steps and 6 Å high double steps.[9] Therefore, it is likely that the alumina films studied in this work also exhibit a stepped morphology instead of an oxide surface with large flat terraces. It has been discussed in the literature that the height of a perfect monoclinic θ-Al_2O_3 unit cell is 11.83 Å,[3] suggesting that the ordered θ-Al_2O_3 films studied here do exhibit some deviations from the ideal θ-Al_2O_3 crystal as their thicknesses are somewhat smaller than the perfect monoclinic unit cell. On the other hand, it will be shown in the coming sections that the θ-Al_2O_3/NiAl(100) surfaces discussed here are still highly ordered and, thus, have a low surface defect density, as is evident from the chemical interaction of these surfaces with H_2O molecules.

The chemical composition of the θ-Al_2O_3/NiAl(100) films was also studied with electron spectroscopies. Figure 2 presents the AES data for a θ-alumina thin film whose thickness was estimated to be 6 ± 2 Å. The prominent features of the spectrum are the KLL features for Al at 39−66 and 1392 eV, the Ni LMM triplet at 713, 779, and 848 eV, and the O KLL peak at 509 eV. The strong O feature in the AES spectra relative to the Ni and Al substrate features suggests that oxidation of the bimetallic NiAl(100) substrate occurs during film growth. A detailed look at the Al KLL region within 39−66 eV in the inset of Figure 2 provides more evidence for this observation. It is clearly seen that after the oxidation process, several well-resolved features are visible at 39, 47, and 55 eV which are attributed to oxidized Al species, Al^{3+}.[5] In addition to these Al^{3+} features, a relatively smaller peak at 66 eV is also present in the inset of Figure 2, which is associated with the metallic Al^0 of the NiAl(100) substrate or the interfacial region below the oxide overlayer. Although the data presented in Figure 2 indicate that the substrate Al atoms are oxidized during the film growth process, it is difficult to extract this sort of information about the oxidation state of the substrate Ni atoms using solely AES.

To address the oxidation states of the surface species in a more detailed fashion, XPS experiments were performed. Figure 3a shows the XPS data corresponding to the Al2p region of the θ-Al_2O_3/NiAl(100) surface. At least three different Al oxidation states are observed with XPS. Deconvolution of the XPS spectrum, given in Figure 3a, reveals that these three distinct features are located at 74.8, 73.1, and 72.3 eV, which are assigned to fully oxidized Al_2O_3, AlO_x suboxides, and metallic Al (i.e., Al^0), respectively.[6,7,24,25] Al species having lower oxidation states than the fully oxidized Al_2O_3 surface, observed after the alumina film growth on NiAl bimetallic substrates, have also been discussed in previous reports, suggesting the presence of a typical AlO_x interfacial environment between the NiAl bimetallic substrate and the Al_2O_3,[6,7,24,25] or the presence of Al atoms with different coordinations (T_h or O_h) in the oxide structure.[25]

Figure 3b shows the Ni2p region of the XPS spectrum for an ordered θ-Al_2O_3 film grown on NiAl(100). Two major features are observed in the Ni2p region at 869.8 and 852.5 eV, which are separated by 17.3 eV. These are the characteristic features for metallic Ni species, more specifically $Ni2p_{1/2}$ and $Ni2p_{3/2}$ peaks that are separated by a typical spin−orbit splitting of 17.3 eV.[26] All of these traits seen in Figure 3b unambiguously imply that Ni atoms of the NiAl(100) substrate are not oxidized during the film growth and therefore segregate to the subsurface and conserve their original metallic oxidation state, in agreement with the previous findings.[6,7,24,25]

3.2. H_2O Adsorption on θ-Al_2O_3/NiAl(100). The chemical reactivity and the defect structure of synthesized θ-Al_2O_3/NiAl(100) films were investigated using water adsorption. As we have discussed above, it is commonly argued that the

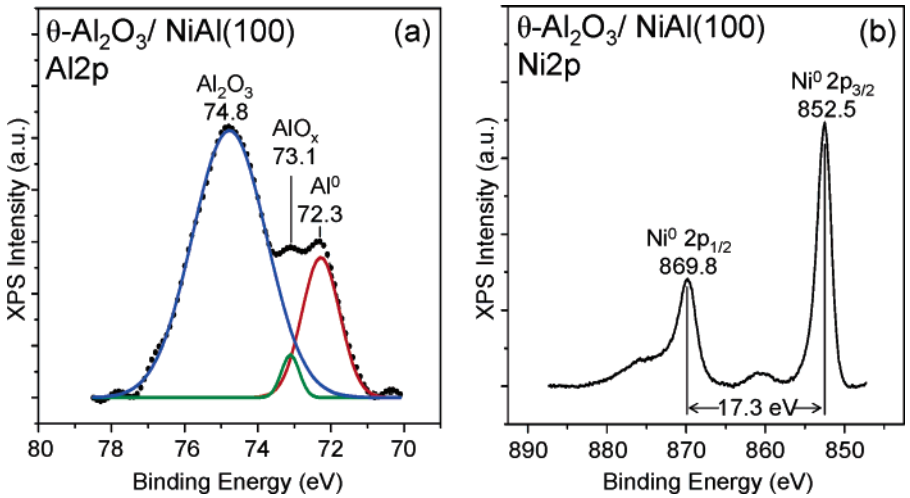

Figure 3. Data corresponding to the (a) Al2p and (b) Ni2p regions of the X-ray photoelectron spectra for θ-Al_2O_3/NiAl(100) ultrathin film obtained using a Mg Kα X-ray source.

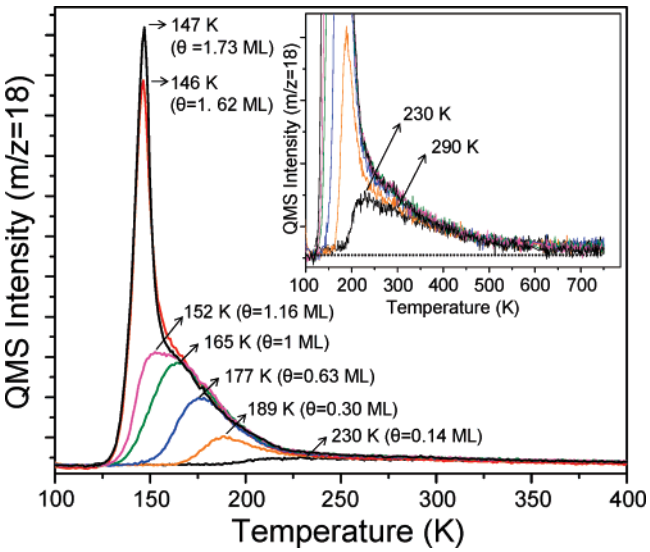

Figure 4. TPD data for H_2O adsorption on an ordered θ-Al_2O_3/NiAl(100) thin film with various surface coverages of water. For each given TPD curve, H_2O was adsorbed on a clean θ-Al_2O_3 film at 100 K to obtain the given coverage values. The inset highlights the water desorption in the high-temperature tail of the TPD traces.

concentration of the defect sites is closely related to the extent of H_2O dissociation and the corresponding hydroxyl formation on the oxide surfaces.[10,11] Therefore, H_2O adsorption was performed on θ-Al_2O_3/NiAl(100) at 100 K and the H_2O desorption characteristics were studied with TPD. Figure 4 presents representative TPD data for H_2O overlayers that are dosed on the θ-Al_2O_3 films at 100 K by varying H_2O adsorbate coverage using a pinhole doser. It should be noted that only a single desorption product (i.e., 18 amu) was observed following water adsorption.

Figure 4 reveals that at low H_2O exposures a single desorption maximum is observed within 230−165 K, which tends to shift to lower temperatures with increasing water exposure. A further increase in the H_2O exposure results in the formation of a second desorption feature in the TPD spectra that can be initially observed as a low-temperature shoulder at 152 K. By monotonically increasing the water exposure to still higher values, a new distinct desorption peak is obtained at 146 K, which slightly shifts to 147 K upon a further increase in H_2O exposure. An important aspect of these distinct desorption traces at 146−147 K that is worth noticing is that they have a common leading edge.

The most significant characteristic of the TPD spectra presented in Figure 4 is that all of the desorption maxima are observed at temperatures below 230 K, independent of the H_2O exposure that is used in the adsorption experiments. This is relatively unexpected because on many oxide surfaces such as α-Al_2O_3(0001),[15,16] MgO(100),[27] Fe_3O_4(111),[28] or α-Cr_2O_3-(0001)[29] a water desorption feature was seen at $T > 250$ K.[11] These higher-temperature desorption features were attributed to the dissociative adsorption of H_2O, and hydroxyl formation on the oxygen atom vacancies. Lack of such a high-temperature desorption peak in the TPD data shown in Figure 4 suggests that H_2O adsorption on the well-ordered θ-Al_2O_3/NiAl(100) surface takes place predominantly in a molecular fashion.

Based on the common interpretation of molecular adsorption of water on oxide surfaces,[10,11] under low coverage conditions H_2O is assigned to adsorb on the Al^{3+} cation sites that are located just below the plane of the surface oxygen layer. These 4-fold surface adsorption sites are still accessible to adsorb isolated water molecules on the θ-Al_2O_3/NiAl(100) surface.

It can be readily seen in Figure 4 that the single desorption maximum at 230 K shifts to lower temperatures until the appearance of a second desorption feature at 152 K. Therefore, increasing H_2O exposure at 100 K monotonically increases the surface coverage of water (the sticking probability of H_2O on solid surfaces at 100 K is unity[10,11]), eventually leading to the completion of the first monolayer (i.e., the coverage corresponding to one H_2O molecule per Al^{3+} site) with a TPD peak maximum at 165 K. This spectrum is used as a reference to estimate H_2O coverages corresponding to the TPD curves in Figure 4. Once the nature of H_2O adsorption is assigned to be molecular, a more detailed analysis of the TPD data is feasible. In the submonolayer adsorption regime, the shift of the desorption maxima to lower temperatures with increasing coverage can not be attributed to a second order (recombinative) desorption behavior as the dominant adsorption type for H_2O is molecular. Rather, the behavior of the desorption maxima for submonolayer water can be attributed instead to a first-order desorption with repulsive interactions between the H_2O molecules, similar to the repulsive interactions observed for H_2O molecules adsorbed on the five coordinated Ti^{4+} rows on TiO_2(110).[30]

In the multilayer regime, the TPD spectra in Figure 4 reveal a common leading edge and a desorption maximum which shifts to higher temperatures with increasing H_2O coverage that fits very well to a zeroth order desorption behavior of hydrogen-bonded ice multilayers from the metal oxide surface.[10,11] It should be noted that the spectrum corresponding to $\theta_{H_2O} = 1.16$ ML exhibits an interesting characteristic that is worth mentioning. Figure 4 reveals that the leading edge of this spectrum does not coincide with the leading edges of the TPD spectra that are obtained for higher H_2O coverages and exhibits a shoulder at 152 K. Therefore, the shoulder observed at 152 K can be attributed to H_2O molecules that are populating anion sites just after the saturation of the cation sites, leading to the formation of three-dimensional bulklike water structures consistent with a cluster nucleation model.

Although water adsorbs predominantly in a molecular fashion on θ-Al_2O_3/NiAl(100), dissociation of H_2O on the small number of defect sites can not be ruled out completely. This phenomenon can be better discussed by analyzing the inset of Figure 4, focusing on the high-temperature tail of the TPD data for H_2O desorption. The inset of Figure 4 shows that the high-temperature tails of the TPD spectra converge to the same trace despite the fact that H_2O coverage is increased more than an order of magnitude, implying that the observed high-temperature features are not due to pumping limitations in the vacuum chamber. A closer inspection of the curve corresponding to $\theta_{H_2O} = 0.14$ ML in the inset reveals that, besides the 230 K feature, which is most likely associated with molecular H_2O desorption, additional features appear starting from 290 K extending up to 650 K, indicating the presence of multiple recombinative H_2O desorption processes due to hydroxyl groups on dissimilar adsorption sites. Furthermore, H_2O desorption features at $T > 300$ K associated with the defect sites are saturated even at the small H_2O coverage of 0.14 ML. The area below these desorption features does not change with increasing coverage, suggesting that H_2O molecules might have enough mobility on the θ-Al_2O_3/NiAl(100) surface at 100 K to preferentially adsorb on the defect sites until they are saturated, which is then followed by the population of molecular H_2O at the Al^{3+} cation sites. The defect density of the θ-Al_2O_3/NiAl(100) surface leading to the small extent of water dissociation can be estimated by integrating the area below the $\theta_{H_2O} = 0.14$ ML curve for T

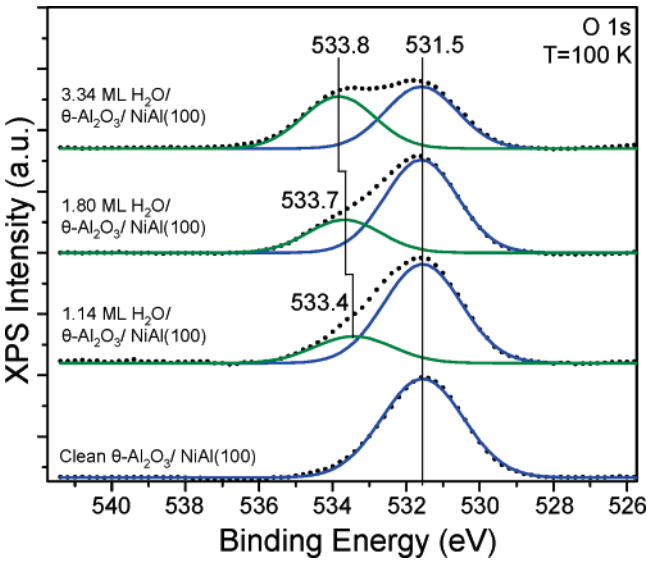

Figure 5. O1s region of the XPS data corresponding to the H_2O adsorption experiments for various water coverages on a θ-Al_2O_3/NiAl(100) thin film. For each XPS spectrum given, H_2O was adsorbed on a clean θ-Al_2O_3 film at 100 K, the XPS spectrum is acquired at 100 K, and then the coverage of the adsorbed H_2O layer was determined by a subsequent TPD experiment.

> 300 K. This yields a coverage of 0.05 ML that is consistent with the high order of the θ-Al_2O_3 film suggested by the LEED data (Figure 1).

H_2O adsorption on the θ-Al_2O_3/NiAl(100) surface was also studied with XPS by varying the surface H_2O coverage. The XPS spectra of Figure 5 compare the O1s region for the clean θ-Al_2O_3/NiAl(100) surface with that for the 1.14, 1.80, and 3.34 ML H_2O overlayers on the oxide film. Figure 5 shows that the O1s peak for the clean alumina film is centered at 531.5 eV. As the film is exposed to H_2O, a shoulder on the high binding energy side of the O1s feature of the clean film starts developing, and its intensity increases monotonically with water coverage. This additional peak at 533.4 eV is associated with the molecularly adsorbed H_2O on the oxide film. Although the position of the O1s feature due to the oxide film stays constant with increasing exposure, that of the adsorbed H_2O related feature shifts slightly to higher binding energies (+0.4 eV). This small binding energy shift has been attributed to the reduced final state screening effects at larger distances from the substrate.[11] It is also apparent from the topmost spectrum in Figure 5 that, as the ice layer becomes thicker, the O1s feature associated with the oxide film attenuates. The single major feature developing in the XPS spectra upon H_2O adsorption also supports our understanding that water adsorption occurs mostly molecularly on the well-ordered oxide surface. The very small amount of dissociation products likely falls below the detection limits of the current experiment due to their expected small intensities and overlap with the much larger O1s features just discussed. It should also be noted that H_2O adsorption was found to have no significant effect on the Ni2p XPS features, and the θ-Al_2O_3/NiAl(100) surface was recovered without any evident change in the film composition (AES) and structure (LEED) after the desorption of water.

Our understanding of the θ-Al_2O_3/NiAl(100) surface structure is summarized in the schematic given in Figure 6, which depicts the topmost surface of the ordered, oxygen-terminated θ-Al_2O_3 film, where underlying Al^{3+} cations form a (2×1, 1×2) structure. Until the completion of the first water monolayer, H_2O prefers to adsorb in a molecular fashion on the Al^{3+} rows

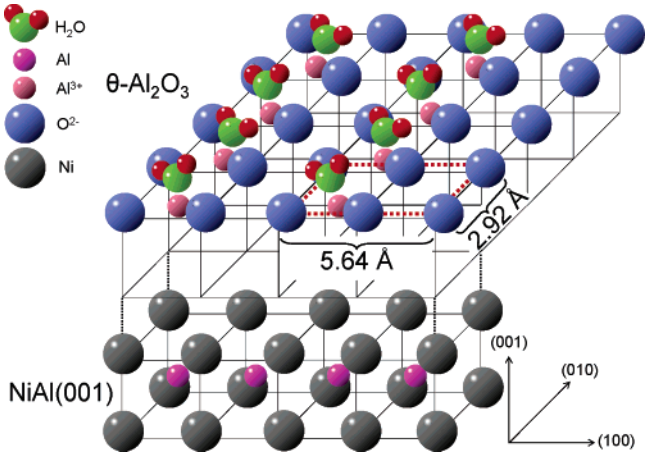

Figure 6. Schematic illustrating the θ-Al_2O_3/NiAl(100) surface structure and the H_2O adsorption on the oxide film at $\theta_{H_2O} \leq 1$ ML. Atomic or ionic sizes are not drawn to scale in the figure. Bond distance values are taken from ref 3 and correspond to the crystal parameters of a bulk θ-Al_2O_3 monoclinic crystal. In a recent STM study, these distances were measured to be (3 Å × 6 Å) and (3 Å × 6.8 Å) for different θ-Al_2O_3 domains, and the Al^{3+} sites were found to be 1.4 Å below the oxygen layer.[31]

which are oriented along the ⟨010⟩ direction with respect to the NiAl(001) substrate. Due to this particular alignment of the adsorbed H_2O molecules up to a monolayer coverage regime, intermolecular hydrogen bonding between the adsorbed water molecules seems to be unlikely at these low coverages. This argument is also supported by the fact that water molecules residing on the Al^{3+} sites are relatively far apart (distances between water molecules along the ⟨010⟩ and ⟨100⟩ directions are ~3 and ~6 Å, respectively), decreasing the possibility of intermolecular hydrogen bonding between the water molecules at low coverages. Therefore, water molecules prefer to densely pack along the ⟨010⟩ direction, which enables strong binding to the Al^{3+} sites. This adsorbed H_2O structure along the Al^{3+} rows of the oxide film is consistent with the observed repulsive interaction in the first monolayer suggested by the current TPD results. As the water coverage exceeds one monolayer, water molecules start populating other adsorption sites (anionic sites) of the θ-Al_2O_3/NiAl(100) surface, which allows the formation of hydrogen-bonded three-dimensional ice networks.

4. Conclusions

The interaction of adsorbed H_2O overlayers with an ordered θ-Al_2O_3 thin film epitaxially grown on NiAl(100) was studied using various surface analysis techniques. Our results can be summarized as follows:

(a) H_2O adsorption on the θ-Al_2O_3/NiAl(100) surface is predominantly molecular rather than dissociative.

(b) For $\theta_{H_2O} < 1$ ML, H_2O molecules populate Al^{3+} cation sites to form isolated H_2O species ordered in rows along the cation sites of the oxide surface. Repulsive interactions between these adsorbed water molecules are indicated by a significant reduction in the desorption temperature with increasing H_2O coverages up to 1 ML.

(c) For $\theta_{H_2O} > 1$ ML, H_2O overlayers were observed to form three-dimensional ice multilayers. Water molecules occupy both cationic and anionic adsorption sites on the oxide surface, allowing the formation of hydrogen bonding in the ice network.

(d) A small extent of H_2O dissociation was observed to occur on the θ-Al_2O_3/NiAl(100) surface, which was attributed to the presence of a low concentration of surface defects. Titration of the defect sites with adsorbed H_2O molecules revealed a defect

density of 0.05 ML for the θ-Al_2O_3/NiAl(100) system consistent with the highly ordered nature of the oxide film suggested by the LEED images.

Acknowledgment. We gratefully acknowledge the U.S. Department of Energy (DOE), Office of Basic Energy Sciences, Division of Chemical Sciences, for support of this work. The research described in this paper was performed at the Environmental Molecular Sciences Laboratory (EMSL), a national scientific user facility sponsored by the DOE Office of Biological and Environmental Research and located at Pacific Northwest National Laboratory (PNNL). PNNL is operated for the U.S. DOE by Battelle Memorial Institute under contract number DE-AC05-76RL01830. We would like to acknowledge with pleasure Drs. Michael A. Henderson, J. M. White, Zdenek Dohnalek, Ja Hun Kwak, and Jooho Kim for fruitful discussions.

References and Notes

(1) Takeuchi, M.; Matsumoto, S. *Top. Catal.* **2004**, *28*, 151.
(2) Taylor, K. C. *Catal. Rev.-Sci. Eng.* **1993**, *35*, 457.
(3) Gassmann, P.; Franchy, R.; Ibach, H. *Surf. Sci.* **1994**, *319*, 95.
(4) Ivey, M. M.; Layman, K. A.; Avoyan, A.; Allen, H. C.; Hemminger, J. C. *J. Phys. Chem. B* **2003**, *107*, 6391.
(5) Gassmann, P.; Franchy, R.; Ibach, H. *J. Electron Spectrosc. Relat. Phenom.* **1993**, *64/65*, 315.
(6) Libuda, J.; Frank, M.; Sandell, A.; Andersson, S.; Bruhwiler, P. A.; Baumer, M.; Martensson, N.; Freund, H. J. *Surf. Sci.* **1997**, *384*, 106.
(7) Tzvetkov, G.; Zubavichus, Y.; Koller, G.; Schmidt, Th.; Heske, C.; Umbach, E.; Grunze, M.; Ramsey, M. G.; Netzer, F. P. *Surf. Sci.* **2003**, *543*, 131.
(8) Young, E. W. A.; de Wit, J. H. W. *Solid State Ionics* **1985**, *16*, 39.
(9) Blum, R. P.; Ahlbehrendt, D.; Niehus, H. *Surf. Sci.* **1998**, *396*, 176.
(10) Thiel, P. A.; Madey, T. E. *Surf. Sci. Rep.* **1987**, *7*, 211.
(11) Henderson, M. A. *Surf. Sci. Rep.* **2002**, *46*, 1.
(12) Layman, K. A.; Hemminger, J. C. *J. Catal.* **2004**, *222*, 207.
(13) Chen, J. G.; Crowell, J. E.; Yates, J. T., Jr. *J. Chem. Phys.* **1986**, *84*, 5906.
(14) Coustet, V.; Jupille, J. *Surf. Sci.* **1994**, *307*−*309*, 1161.
(15) Nelson, C. E.; Elam, J. W.; Cameron, M. A.; Tolbert, M. A.; George, S. M. *Surf. Sci.* **1998**, *416*, 341.
(16) Elam, J. W.; Nelson, C. E.; Cameron, M. A.; Tolbert, M. A.; George, S. M. *J. Phys. Chem. B* **1998**, *102*, 7008.
(17) Liu, P.; Kendelewicz, T.; Brown, G. E., Jr.; Nelson, E. J.; Chambers, S. A. *Surf. Sci.* **1998**, *417*, 53.
(18) Frederick, B. G.; Apai, G.; Rhodin, T. N. *Surf. Sci.* **1991**, *244*, 67.
(19) Qin, F.; Magtoto, N. P.; Kelber, J. A. *Surf. Sci.* **2004**, *565*, L277.
(20) Powell, C. J.; Jablonski, A. *Surf. Sci.* **2001**, *488*, L547.
(21) Wu, M. C.; Oh, W. S.; Goodman, D. W. *Surf. Sci.* **1995**, *330*, 61.
(22) Chen, P. J.; Colaianni, M. L.; Yates, J. T. *Phys. Rev. B* **1990**, *41*, 8025.
(23) Rodriguez, J. A.; Kuhn, M.; Hrbek, J. *J. Phys. Chem.* **1996**, *100*, 18240.
(24) Fremy, N.; Maurice, V.; Marcus, P. *Surf. Interface Anal.* **2002**, *34*, 519.
(25) Jaeger, R. M.; Kuhlenbeck, H.; Freund, H. J.; Wuttig, M.; Hoffmann, W.; Franchy, R.; Ibach, H. **1991**, *259*, 235.
(26) Wagner, C. D.; Riggs, W. M.; Davis, L. E.; Moulder, J. F.; Muilenberg, G. E. *Handbook of X-ray Photoelectron Spectroscopy*; Eden Prairie, MN, 1979.
(27) Stirniman, M. J.; Huang, C.; Smith, R. S.; Joyce, S. A.; Kay, B. D. *J. Chem. Phys.* **1996**, *105*, 1295.
(28) Joseph, Y.; Kuhrs, C.; Ranke, W.; Ritter, M.; Weiss, W. *Chem. Phys. Lett.* **1999**, *314*, 195.
(29) Henderson, M. A.; Chambers, S. A. *Surf. Sci.* **2000**, *449*, 135.
(30) Henderson, M. A. *Surf. Sci.* **1996**, *355*, 151.
(31) Fremy, N.; Maurice, V.; Marcus, P. *J. Am. Ceram. Soc.* **2003**, *86*, 669.